PERGAMON

International Journal of Solids and Structures 38 (2001) 3111–3126

INTERNATIONAL JOURNAL OF SOLIDS and STRUCTURES

www.elsevier.com/locate/ijsolstr

Damage assessment of structures using modal test data

N. Hu [a,*], X. Wang [b], H. Fukunaga [a], Z.H. Yao [b], H.X. Zhang [c], Z.S. Wu [d]

[a] *Department of Aeronautics and Space Engineering, Tohoku University, 01 Aramaki-Aoba, Aoba-ku, Sendai 980-8579, Japan*
[b] *Department of Engineering Mechanics, Tsinghua University, Beijing 100084, People's Republic of China*
[c] *Department of Oil Mechanical Engineering, Institute of Chongqing Logistics Engineering, Chongqing 400016, People's Republic of China*
[d] *Department of Urban and Civil Engineering, Ibaraki University, Mito 310, Japan*

Received 4 August 1999; in revised form 29 June 2000

Abstract

System health monitoring of structures is important not only for conducting safe operation but also maintaining system performance. In this paper, two identification algorithms for assessing structural damages using the modal test data have been developed. An important characteristic in the present approaches is that the employment of the global numerical models (e.g. FEM model) and some important information (e.g. Young's modulus) of structures are avoided to a great extent. As the first step of the damage identification, two algorithms for the detection of damage location are proposed, which are similar in concept to the subspace rotation algorithm or best achievable eigenvector technique. Furthermore, a quadratic programming model is set up for the two approaches to predict the damage extent. To demonstrate the capability of the proposed approaches, an example of a 10-bay planar truss structure is employed for checking the present approaches numerically. Furthermore, the experimental data from the vibration test of a beam with two fixed ends are used directly in the present approaches. The final results show that the present techniques perform quite well in spite of the little structural information and measurement inaccuracies.

Keywords: Damage detection; Modal analysis; Subspace rotation; Quadratic programming

1. Introduction

Recently, structural damage identification based on vibration monitoring techniques has been paid much attention. Various damage identification algorithms have been developed for dealing with three key problems, i.e. detection of the presence of damages, detection of the structural damage locations and estimation of the damage extents. For the last two problems stated above, most of the existing methods can be thought of as a two-stage algorithm in which damage locations are detected at first, and then damage extents are estimated. Generally, the first step may be more important, but probably more difficult. In the following section, we will review some representative algorithms in this field.

* Corresponding author. Fax: +81-22-217-6995.
E-mail address: hu@ssl.mech.tohoku.ac.jp (N. Hu).

0020-7683/01/$ - see front matter
PII: S0020-7683(00)00292-4

For the damage detection problem, Chen and Garba (1988) calculated the residual force vectors. By picking out the degrees of freedom (DOFs) with non-zero components in the residual force vectors, the damage locations can be identified. Ricles and Kosmatka (1992) employed the same methodology by further considering the variation of the mass matrix due to damages. By employing control-based eigenstructure assignment techniques, a subspace rotation algorithm was proposed by Zimmerman and Kaouk (1992), in which the damage vector and relative rotation angle are used to identify the DOFs affected by damage. Lim and Kashangaki (1994) and Lim (1995) put forward a similar method in concept using best-achievable eigenvectors, however, to identify the damaged structural members directly. Another important and interesting category uses the characteristics of the flexibility matrix. Unlike the stiffness matrix, the flexibility matrix can be formed more accurately through the usage of first several order experimental modal data. Lin (1995) used this flexibility matrix to multiply the pre-damaged FEM stiffness matrix to determine the damage locations. Pandey and Biswas (1994) detected the damage locations through the variation of the flexibility matrices before and after damage. More recent work in this area includes those proposed by Peterson et al. (1995), Park and Alvin (1996) and Fukunaga et al. (in press). An important advantage in this category is that the usage of the analytical model can be avoided. Also, some researchers used some special information such as curvature modes (Pandey et al., 1991) and strain data (Kahl and Sirkis, 1996) to search for the damage locations.

For the estimation of damage extent, one important class of methods for correlating measured modal data with analytical finite element models is the minimization or elimination of model force error. This error is that resulting from the substitution of the analytical FEM and the measured modal data into the structural eigenproblem. Various approaches have been presented to minimize some measure of the error in the eigenproblem by perturbing the baseline values in the analytical model, such as the components of the stiffness, damping, and mass matrices. One type of method, known as sensitivity-based model update, uses the sensitivities of the modal response parameters of the FEM (such as modal frequencies and mode shapes) to the structural design parameters (such as Young's modulus, density, etc.) to iteratively minimize the modal force error (Ricles and Kosmatka, 1992). Another type of method, known as eigenstructure assignment, designs a controller that minimizes the modal force error (Lim, 1995). Further, another type of method, known as optimal matrix update, solves a closed-form equation for the matrix perturbations that minimize the modal force error or constrain the solution to satisfy it (Chen and Garba, 1988; Kaouk and Zimmerman, 1994). For a detailed understanding of the work in this field, one can refer the review papers by Hajela and Soeiro (1990) and Zimmerman and Smith (1992).

Although there has been much development in this area, as to practical applications, many difficulties should be overcome, such as the measurement uncertainty and inadequate test data, etc. Also, another important difficulty stems from the difference between the analytical models and real structures. Generally, the error in analytical model may be classified into the following several aspects: (1) approximation in boundary conditions of analytical models may make the analytical stiffness matrix deviate from the practical one, (2) connectivity conditions of elements in analytical models cannot reflect the real connective state of structural members, (3) some important material parameters in analytical models, e.g. Young's modulus, may not represent the real ones, (4) there are many stiffness sources in practical structures, which are ignored in analytical models due to computational capacity and (5) the coarse mesh or unsuitable element types can cause the errors in analytical models. Actually, for complex structures, no reasonable analytical models can be evaluated.

Most of the approaches mentioned previously, except for those using the flexibility matrix [2 9 11 12], however, employ the analytical models. For the practical applications, it may be more attractive to avoid employing too much information of the analytical models. Hence, two kinds of algorithms are presented in this paper, which are not dependent on analytical models so strongly. It is hoped that this paper can shed light on the damage assessment problem. In the first algorithm, the employment of the analytical global stiffness and mass matrices are avoided by using a special perturbation technique, which leads to ap-

proximate estimation of the damage extent. In the second one, only analytical mass matrix is employed, which is completely accurate for the prediction of damage extent.

2. Theory

2.1. Identification of damage location

In the following, two algorithms are described in detail. For the first one, the analytical global stiffness and mass matrices are not needed, which will be cited as DDNKM for brevity. For the second one, only the analytical mass matrix is employed in damage identification process, which is named as DDNK.

Consider the free vibration of a linear n DOF system, which is described as

$$\mathbf{K}\mathbf{\Phi} = \mathbf{M}\mathbf{\Phi}\mathbf{\Lambda} \tag{1}$$

with the symmetric stiffness and mass matrices $\mathbf{K}, \mathbf{M} \in \mathbb{R}^{n\times n}$, $\mathbf{\Phi}$, a $n \times m$ modal matrix, and $\mathbf{\Lambda} = \mathrm{diag}\{\lambda_i; i = 1, \ldots, m\}$, the eigenvalue matrices, which represent the truncated modal test results (m-order). We refer system (1) as the *pre-damaged system*. This system is subject to changes caused by the damages. Suppose the *damaged system* is characterized as

$$(\mathbf{K} + \Delta\mathbf{K})\mathbf{\Phi}^* = \mathbf{M}\mathbf{\Phi}^*\mathbf{\Lambda}^*, \tag{2}$$

where no variation in the mass matrix due to damage is assumed, and the variation of structural stiffness matrix is $\Delta\mathbf{K} \in \mathbb{R}^{n\times n}$. Also, $\mathbf{\Lambda}^* = \mathrm{diag}\{\lambda_i^*; i = 1, \ldots, m\}$ and $\mathbf{\Phi}^* \in \mathbb{R}^{n\times m}$ are the truncated test eigenvalue and eigenmode matrices of the damaged structures.

The following Rayleigh–Ritz approximation $\mathbf{\Phi}^* \approx \mathbf{\Phi}\mathbf{\Gamma}$ with the assumption of $\mathbf{\Phi}^* \in \mathrm{span}\{\mathbf{\Phi}\}$ and $\mathbf{\Gamma} \in \mathbb{R}^{m\times m}$ is employed. Both the sides of Eq. (2) are multiplied by $(\mathbf{\Phi}\mathbf{\Gamma})^{\mathrm{T}}$ simultaneously, and using the following conditions:

$$\mathbf{\Phi}^{\mathrm{T}}\mathbf{K}\mathbf{\Phi} = \mathbf{\Lambda}, \tag{3a}$$

$$\mathbf{\Phi}^{\mathrm{T}}\mathbf{M}\mathbf{\Phi} = \mathbf{I}, \tag{3b}$$

$$\mathbf{\Phi}^{*\mathrm{T}}\mathbf{M}\mathbf{\Phi}^* = \mathbf{\Gamma}^{\mathrm{T}}\mathbf{\Phi}^{\mathrm{T}}\mathbf{M}\mathbf{\Phi}\mathbf{\Gamma} = \mathbf{\Gamma}^{\mathrm{T}}\mathbf{\Gamma} = \mathbf{I}, \tag{3c}$$

where $\mathbf{I}$ and $\mathbf{\Lambda} \in \mathbb{R}^{m\times m}$.

Then, Eq. (2) can be expressed as

$$(\mathbf{\Phi}\mathbf{\Gamma})^{\mathrm{T}}\Delta\mathbf{K}(\mathbf{\Phi}\mathbf{\Gamma}) = \mathbf{\Lambda}^* - \mathbf{\Gamma}^{\mathrm{T}}\mathbf{\Lambda}\mathbf{\Gamma}, \tag{4}$$

where the use of the particular subspace spanned by the columns of matrix $\mathbf{\Phi}$ enables one to employ the bi-orthogonal relations (3a) and (3b). This circumvents the difficulty that neither $\mathbf{K}$ nor $\mathbf{M}$ is known. Thus, the requirement that $\mathbf{\Phi}^* \in \mathrm{span}\{\mathbf{\Phi}\}$ is essential, which can guarantee the obtained $\mathbf{\Lambda}^* = \mathrm{diag}\{\lambda_i^*; i = 1, \ldots, m\}$ and $\mathbf{\Phi}^* \in \mathbb{R}^{n\times m}$ to follow the proposition: $\min \|\mathbf{M}^{1/2}[(\mathbf{K} + \Delta\mathbf{K})\mathbf{\Phi}^* - \mathbf{M}\mathbf{\Phi}^*\mathbf{\Lambda}^*]\|_{\mathrm{F}}$ s.t. $\mathbf{\Phi}^{*\mathrm{T}}\mathbf{M}\mathbf{\Phi}^* = I$ (Ram and Braun, 1991).

Also, it should be mentioned that Eqs. (3a) and (3b) may not be satisfied if $\mathbf{K}$ and $\mathbf{M}$ are analytical matrices. However, here $\mathbf{K}$ and $\mathbf{M}$ are considered as the stiffness and mass of the practical structure. In fact, in the practical vibration test, Eqs. (3a) and (3b) are generally used for obtaining the modal data from the frequency response function curves.

By observing Eq. (4), it can be found that the left-hand side denotes the modal strain energy due to the stiffness variation and the right-hand side mainly represents the variation in natural frequencies and modes. With the vibration modes of intact and damaged structures obtained from modal test, the following least-square technique is used to obtain $\mathbf{\Gamma}$ matrix,

$$\min \|\mathbf{\Phi}\mathbf{\Gamma}_i - \mathbf{\Phi}_i^*\|_2, \quad i = 1, 2, \ldots, m, \tag{5}$$

where $\mathbf{\Phi}_i^*$ and $\mathbf{\Gamma}_i$ denote the ith column of $\mathbf{\Phi}^*$ and $\mathbf{\Gamma}$ matrices, respectively, m is the number of measured natural frequencies and modes from experiment. Consequently, the right-hand side of Eq. (4) can be determined completely from the modal test data.

Another choice is to use the analytical mass matrix only, i.e. DDNK. In general, the mass matrix is not influenced so seriously by boundary constraint, connectivity conditions and material properties as the stiffness matrix. As done by many other authors, it is assumed that the mass matrix is known. In this case, the problem can be solved directly. For the damaged structure, both sides of vibration equation (2) are multiplied by $\mathbf{\Phi}^{\mathrm{T}}$, and using the following relation $\mathbf{\Phi}^{\mathrm{T}}\mathbf{K} = \mathbf{\Lambda}\mathbf{\Phi}^{\mathrm{T}}\mathbf{M}$, the following equation can be obtained:

$$\mathbf{\Phi}^{\mathrm{T}}\Delta\mathbf{K}\mathbf{\Phi}^* = \mathbf{\Phi}^{\mathrm{T}}\mathbf{M}\mathbf{\Phi}^*\mathbf{\Lambda}^* - \mathbf{\Lambda}\mathbf{\Phi}^{\mathrm{T}}\mathbf{M}\mathbf{\Phi}^*. \tag{6}$$

From Eq. (6), it can be found that the right-hand side is completely determined by the experimental data and the analytical mass matrix, and the left-hand side is dominated by the stiffness variation. Also, unlike Eq. (4), Eq. (6) is theoretically exact.

After obtaining Eqs. (4) and (6) for two approaches, we can set up our identification algorithm. Usually, in the left-hand sides of Eqs. (4) and (6), the unknown stiffness variation can be written in the form of the elemental stiffness variations as

$$\Delta\mathbf{K} = \sum_{i=1}^{\mathrm{ND}} \mathbf{B}_i^{\mathrm{T}}\,\Delta\mathbf{k}_i^*\,\mathbf{B}_i, \tag{7}$$

where ND is the number of damaged elements, $\Delta\mathbf{k}_i^* \in \mathbb{R}^{k\times k}$ is the stiffness variation in the ith element of k DOFs and $\mathbf{B}_i \in \mathbb{R}^{k\times n}$ is the Boolean matrix of the ith element.

Furthermore, the matrix $\Delta\mathbf{k}_i^*$ can be written in the following form:

$$\Delta\mathbf{k}_i^* = \alpha_i E_i\,\Delta\mathbf{k}_i, \tag{8}$$

where α_i is the damage fraction value or damage extent of material stiffness properties, E_i is a parameter representing the undamaged material stiffness property in the ith element, which is usually unknown. In addition, $\Delta\mathbf{k}_i$ is a matrix of the form of the ith element stiffness matrix containing only geometric quantities or terms containing Poisson's ratio possibly. This matrix should time -1 to denote the stiffness reduction due to damage.

If the finite element method or other numerical methods are employed to describe the matrix $\Delta\mathbf{k}_i$, it should be noted that $\Delta\mathbf{k}_i$ can be represented by those elements which can describe bending, torsional, axial and shear behaviors, etc. Also, damage fraction α_i satisfies $0.0 \leqslant \alpha_i \leqslant 1$, where $\alpha_i = 0$ corresponds to an undamaged state, whereas $\alpha_i = 1$ corresponds to a complete loss of stiffness. Referring to Eqs. (6) and (7), and the following definitions,

$$\mathbf{\Psi}_i = \mathbf{B}_i\mathbf{\Phi}, \qquad \mathbf{\Psi}_i^* = \mathbf{B}_i\mathbf{\Phi}^*, \tag{9}$$

where $\mathbf{\Psi}_i \in \mathbb{R}^{k\times m}$ and $\mathbf{\Psi}_i^* \in \mathbb{R}^{k\times m}$ are matrices containing m vectors which possess the components of vibration modes on all DOFs in the ith element.

Finally, Eqs. (4) and (6) can be expressed as follows:

$$\sum_{i=1}^{\mathrm{ND}} \alpha_i E_i(\mathbf{\Gamma}^{\mathrm{T}}\mathbf{\Psi}_i^{\mathrm{T}}\,\Delta\mathbf{k}_i\,\mathbf{\Psi}_i\mathbf{\Gamma}) = \mathbf{\Lambda}^* - \mathbf{\Gamma}^{\mathrm{T}}\mathbf{\Lambda}\mathbf{\Gamma}, \tag{10}$$

$$\sum_{i=1}^{\mathrm{ND}} \alpha_i E_i \boldsymbol{\Psi}_i^{\mathrm{T}} \Delta \mathbf{k}_i \boldsymbol{\Psi}_i^* = \boldsymbol{\Phi}^{\mathrm{T}} \mathbf{M} \boldsymbol{\Phi}^* \boldsymbol{\Lambda}^* - \boldsymbol{\Lambda} \boldsymbol{\Phi}^{\mathrm{T}} \mathbf{M} \boldsymbol{\Phi}^*. \tag{11}$$

The left-hand sides of Eqs. (10) and (11) are expressions of summation of all damaged elements, and then there may also be some errors in $\Delta \mathbf{k}_i^*$ caused by numerical techniques. For simplicity, the possible structural elements are checked one by one. For the ith element only, the following matrix is defined from Eq. (10) for DDNKM

$$\mathbf{L}_i = \alpha_i E_i (\boldsymbol{\Gamma}^{\mathrm{T}} \boldsymbol{\Psi}_i^{\mathrm{T}} \Delta \mathbf{k}_i \boldsymbol{\Psi}_i \boldsymbol{\Gamma}). \tag{12}$$

For Eq. (11), i.e. DDNK,

$$\mathbf{L}_i = \alpha_i E_i (\boldsymbol{\Psi}_i^{\mathrm{T}} \Delta \mathbf{k}_i \boldsymbol{\Psi}_i^*), \tag{13}$$

where $\mathbf{L}_i$ is a $m \times m$ matrix.

Furthermore, the right-hand side of Eq. (10) can be defined as

$$\mathbf{T} = \boldsymbol{\Lambda}^* - \boldsymbol{\Gamma}^{\mathrm{T}} \boldsymbol{\Lambda} \boldsymbol{\Gamma}. \tag{14}$$

Similarly, the right-hand side of Eq. (11) for DDNK can be written as

$$\mathbf{T} = \boldsymbol{\Phi}^{\mathrm{T}} \mathbf{M} \boldsymbol{\Phi}^* \boldsymbol{\Lambda}^* - \boldsymbol{\Lambda} \boldsymbol{\Phi}^{\mathrm{T}} \mathbf{M} \boldsymbol{\Phi}^*, \tag{15}$$

where $\mathbf{T}$ is a $m \times m$ matrix determined by experimental data and mass matrix completely.

Here, to perform the identification of damage location directly using Eq. (10) or Eq. (11), a potential drawback is that there is only very little information in two matrices $\mathbf{L}_i \in \mathbb{R}^{m \times m}$ and $\mathbf{T} \in \mathbb{R}^{m \times m}$, although each row or column is independent of other rows and columns. As will be stated later, only relative rotation angles are evaluated to locate the damage site, hence the matrices $\mathbf{L}_i$ and $\mathbf{T}$ can be enlarged by employing the pre-damaged vibration mode

$$\mathbf{H}_i = \boldsymbol{\Phi} \mathbf{L}_i, \quad \mathbf{F} = \boldsymbol{\Phi} \mathbf{T}. \tag{16}$$

In this case, $\mathbf{H}_i$ and $\mathbf{F}$ are $n \times m$ matrices, which can be partitioned into the following form:

$$\mathbf{H}_i = \begin{bmatrix} \mathbf{H}_i^1 & \mathbf{H}_i^2 & \cdots & \mathbf{H}_i^n \end{bmatrix}^{\mathrm{T}}, \qquad \mathbf{F} = \begin{bmatrix} \mathbf{F}^1 & \mathbf{F}^2 & \cdots & \mathbf{F}^n \end{bmatrix}^{\mathrm{T}}, \tag{17}$$

where $\mathbf{H}_i^j \in \mathbb{R}^{1 \times m}$ and $\mathbf{F}^j \in \mathbb{R}^{1 \times m}$ are the jth row of matrices $\mathbf{H}_i$ and $\mathbf{F}$, respectively.

In addition, it can be found that the left-hand sides of Eqs. (10) and (11) are functions of damage extent α_i, material property E_i and damage site (i.e. Boolean matrix $\mathbf{B}_i$). Therefore, if one tries to use Eqs. (10) and (11) to carry out the damage detection, the influence of damage extent and unknown material property should be removed. By observing Eqs. (12) and (13), it can be found that all components in the matrix $\mathbf{H}_i$ are directly proportional to α_i and E_i. Therefore, the matrix $\mathbf{H}_i$ can be further written in the following form:

$$\begin{bmatrix} \mathbf{H}_i^1 & \mathbf{H}_i^2 & \cdots & \mathbf{H}_i^n \end{bmatrix}^{\mathrm{T}} = \alpha_i E_i \begin{bmatrix} \mathbf{H}_i^{1^*} & \mathbf{H}_i^{2^*} & \cdots & \mathbf{H}_i^{n^*} \end{bmatrix}^{\mathrm{T}}. \tag{18}$$

Hence, there are only some geometric quantities of the ith element in vector $\mathbf{H}_i^{j^*}$.

Finally, the influence of α_i and E_i can be eliminated easily through calculating the angles between vectors $\mathbf{H}_i^j$ and $\mathbf{F}^j (j = 1, 2, \ldots, n)$ as follows:

$$\begin{aligned} \theta_i^j &= \frac{180}{\pi} \cos^{-1} \left(\frac{\mathbf{H}_i^j \mathbf{F}^{j^{\mathrm{T}}}}{\|\mathbf{H}_i^j\|_{\mathrm{F}} \|\mathbf{F}^j\|_{\mathrm{F}}} \right) = \frac{180}{\pi} \cos^{-1} \left(\frac{\alpha_i E_i \mathbf{H}_i^{j^*} \mathbf{F}^{j^{\mathrm{T}}}}{\alpha_i E_i \|\mathbf{H}_i^{j^*}\|_{\mathrm{F}} \|\mathbf{F}^i\|_{\mathrm{F}}} \right) \\ &= \frac{180}{\pi} \cos^{-1} \left(\frac{\mathbf{H}_i^{j^*} \mathbf{F}^{j^{\mathrm{T}}}}{\|\mathbf{H}_i^{j^*}\|_{\mathrm{F}} \|\mathbf{F}^j\|_{\mathrm{F}}} \right), \end{aligned} \tag{19}$$

where $\|\bullet\|_{\mathrm{F}}$ denotes Frebenius norm.

From Eqs. (10) and (11), it can be found that every θ_i^j $(j = 1, 2, \ldots, n)$ should be equal to zero, if the single damage exists in the ith element actually. It means that the directions of vectors $\mathbf{H}_i^j$ and $\mathbf{F}^j$ $(j = 1, 2, \ldots, n)$ are identical, although their lengths may be different by noting the influence of α_i and E_i in vector $\mathbf{H}_i^j$. We can further evaluate the average mean square deviation between θ_i^j $(j = 1, 2, \ldots, n)$ and zero vector in the ith element as follows:

$$R_i = \sqrt{\left(\sum_{j=1}^{n} \theta_i^{j^2}\right) \Big/ n}. \tag{20}$$

If R_i is very small, the possibility of damage in the ith element is large. Further, the average value of R_i for NE possible damaged elements is defined as

$$G = \max\{|R_1|, |R_2|, \ldots, |R_{\mathrm{NE}}|\}. \tag{21}$$

Finally, the following normalized damage index is defined to judge the existence of damage,

$$D_i = 1 - \frac{R_i}{G} \quad (i = 1, 2, \ldots, \mathrm{NE}), \tag{22}$$

where NE is the total number of possible damaged elements. Then, when D_i is large, it can be thought that the possibility of damage in the ith element is very high.

An important characteristic of the present algorithms is that the analytical model, at least the system stiffness matrix, is not used, and the important unknown material parameters are eliminated. A suspicious point is that there may be several structural members, which play a similar role in the variation of first several order natural vibration quantities due to damage. This worry may be true; however, it can be argued that the influence of each structural member on the structural vibration is unique by observing the Boolean matrix $\mathbf{B}_i$ in Eqs. (9)–(11). This matrix is completely determined by the topology of structural members and cannot be the same for different structural members.

A merit in the present algorithms is that the structural members is checked one by one, hence one can select some critical members for structural safety or doubtful members as candidates only, which accelerates the detection process. When all members in structures are selected as candidates, one may doubt that this method is similar in using the global analytical model to those previous methods, since in this case, the global stiffness matrix can be assembled easily. However, by referring to Eqs. (7), (10) and (11), the errors introduced in the usual global analytical model through the description of boundary constraint conditions and elemental connectivity conditions by some artificial means (e.g. assembling techniques for forming the global stiffness matrix) is minimized. The errors in $\mathbf{\Delta K}$ in the left-hand sides of Eqs. (10) and (11) are very small, since only limited elements are damaged and consequently $\mathrm{rank}(\mathbf{\Delta K}) \ll \mathrm{rank}(\mathbf{K})$.

For practical applications, one problem is that only part of structural DOFs can be measured in the vibration modes. In the previous researches using analytical models, this difficulty is overcome by employing condensation techniques, such as Guyan reduction (Kahl and Sirkis, 1996) or modal expansion techniques. Although it is impossible to use these techniques in the present algorithms due to no analytical models, there is no fundamental difficulty to detect the damage locations directly by employing the incomplete measured modes to replace $\mathbf{\Phi}$ and $\mathbf{\Phi}^*$ in Eq. (9). By inspecting the Boolean matrix in Eqs. (4) and (6), the responses at the DOFs, which are related to all candidate members, are usually needed.

2.2. Estimation of damage extent

When the possible damaged members are detected by employing the algorithm described above. The estimation of damage extent is the next important step. It is hoped that the non-damaged members in the

possible damaged members detected previously can be removed. Furthermore, the investigation of damage extent in damaged members can provide some important information about the safety of structures.

If there are NP possible damaged members detected in the first detection step, from Eqs. (10)–(15), it can be obtained that

$$\mathbf{L} = \sum_{i=1}^{\mathrm{NP}} \alpha_i \mathbf{Z}_i = \mathbf{T}, \tag{23}$$

where $\mathbf{Z}_i$ can be expressed for two presented algorithms, respectively.

For DDNKM,

$$\mathbf{Z}_i = E_i(\mathbf{\Gamma}^{\mathrm{T}}\mathbf{\Psi}_i^{\mathrm{T}}\Delta\mathbf{k}_i\mathbf{\Psi}_i\mathbf{\Gamma}). \tag{24}$$

And for DDNK,

$$\mathbf{Z}_i = E_i(\mathbf{\Psi}_i^{\mathrm{T}}\Delta\mathbf{k}_i\mathbf{\Psi}_i^{*}). \tag{25}$$

By employing the least-square method, the following optimization model can be established

$$\begin{aligned} \min \quad & \sum_{i=1}^{\mathrm{NP}}\sum_{j=1}^{n}\sum_{k=1}^{n}(\alpha_i Z_i^{jk} - T^{jk})^2 \\ \text{s.t.} \quad & \alpha_i \leqslant 1, \\ & \alpha_i \geqslant 0. \end{aligned} \tag{26}$$

The above model can further be cast into the following quadratic programming problem for determining the damage extent α_i,

$$\begin{aligned} \min \quad & f(\boldsymbol{\alpha}) = \tfrac{1}{2}\boldsymbol{\alpha}^{\mathrm{T}}\mathbf{A}\boldsymbol{\alpha} + \mathbf{C}^{\mathrm{T}}\boldsymbol{\alpha} + D \\ \text{s.t.} \quad & \mathbf{I}\boldsymbol{\alpha} \leqslant \mathbf{d}, \\ & \mathbf{I}\boldsymbol{\alpha} \geqslant \mathbf{0}, \end{aligned} \tag{27}$$

where

$$\boldsymbol{\alpha} = \{\, \alpha_1 \quad \alpha_2 \quad \cdots \quad \alpha_{\mathrm{NP}} \,\}, \tag{28a}$$

$$\mathbf{A} = \begin{bmatrix} \sum_{j=1}^{n}\sum_{k=1}^{n} Z_1^{jk^2} & \sum_{j=1}^{n}\sum_{k=1}^{n} Z_1^{jk} Z_2^{jk} & \cdots & \sum_{j=1}^{n}\sum_{k=1}^{n} Z_1^{jk} Z_{\mathrm{NP}}^{jk} \\ \sum_{j=1}^{n}\sum_{k=1}^{n} Z_2^{jk} Z_1^{jk} & \sum_{j=1}^{n}\sum_{k=1}^{n} Z_2^{jk^2} & \cdots & \sum_{j=1}^{n}\sum_{k=1}^{n} Z_2^{jk} Z_{\mathrm{NP}}^{jk} \\ \vdots & \vdots & \vdots & \vdots \\ \sum_{j=1}^{n}\sum_{k=1}^{n} Z_{\mathrm{NP}}^{jk} Z_1^{jk} & \sum_{j=1}^{n}\sum_{k=1}^{n} Z_{\mathrm{NP}}^{jk} Z_{21}^{jk} & \cdots & \sum_{j=1}^{n}\sum_{k=1}^{n} Z_{\mathrm{NP}}^{jk^2} \end{bmatrix}, \tag{28b}$$

$$\mathbf{C}^{\mathrm{T}} = \left\{ -\sum_{j=1}^{n}\sum_{k=1}^{n} Z_1^{jk} T^{jk} \quad -\sum_{j=1}^{n}\sum_{k=1}^{n} Z_2^{jk} T^{jk} \quad \cdots \quad -\sum_{j=1}^{n}\sum_{k=1}^{n} Z_{\mathrm{NP}}^{jk} T^{jk} \right\}, \tag{28c}$$

$$D = \sum_{j=1}^{n}\sum_{k=1}^{n} T_{jk}^2, \tag{28d}$$

and $\mathbf{d}$, $\mathbf{0}$ and $\mathbf{I}$ are unit, zero vectors and unit matrix, respectively.

The merits of the above quadratic programming model can be mentioned as (1) The feasible domain is convex due to linear constraint conditions. If $\mathbf{A}$ matrix is semi-positive, the objective function is convex. Consequently, there is a unique solution in this problem. (2) The computational amount is small due to no

computation of sensitivity information. Also, by inspecting Eqs. (27) and (28), it can be found that the number of the equations in a dual problem constructed from this quadratic programming model is only 2 NP, and usually NP is very small after the first step. This quadratic programming problem can be solved by employing many existing successful algorithms, such as Lemke algorithm, etc. Here, the algorithm presented by Goldfarb and Idnani (1983) is adopted to deal with this problem. Furthermore, this quadratic programming model is theoretically accurate for DDNK.

It should be pointed out that the damage detection algorithm in Section 2.1 is constructed based on the assumption of the single damage case. Hence, the present algorithms may be incapable to tackle the multiple damage case. It is very difficult to overcome this inefficiency completely; however, a remedial measure can be taken. In usual cases, although all damaged members cannot be detected at the same time, some important or seriously damaged structural members can always be detected in the first step by using the damage detection algorithm in Section 2.1. Then, the damage extent can be calculated from the algorithm proposed in Section 2.2. By eliminating the influence of these identified damaged members from the right-hand sides of Eqs. (10) and (11), e.g.

$$\sum_{i=1}^{\mathrm{NDR}} \alpha_i E_i \boldsymbol{\Psi}_i^{\mathrm{T}} \Delta \mathbf{k}_i \boldsymbol{\Psi}_i^* = \mathbf{T} - \sum_{j=1}^{\mathrm{NDF}} \alpha_j E_j \boldsymbol{\Psi}_j^{\mathrm{T}} \Delta \mathbf{k}_j \boldsymbol{\Psi}_i^*, \tag{29}$$

where the number of identified damaged members in the previous step is NDF, and the number of the damaged members undetected yet is NDR. Then, the undetected damaged members may be found using the algorithm in Section 2.1 by employing the right-hand side of Eq. (29) as a new **T** matrix. Naturally, the feasibility of this step is dependent on the accuracy of the damage extents obtained in the first step, so only DDNK should be used.

3. Verifications

3.1. Planar truss structure

A 10-bay planar truss shown in Fig. 1 is used in implementing the damage identification methods described above. The FEM analysis is used to simulate the experimental data. The lumped-mass representation is adopted to generate the mass matrix. Total numbers of elements and nodes are 41 and 22, respectively. The dimensions of the truss are shown in Fig. 1. The truss is constructed from carbon-fiber-reinforced-plastic truss members, whose material constants are listed as follows:

$$E = 42.4\ \mathrm{GPa}, \qquad A = 1 \times 10^{-3}\ \mathrm{m}^2, \qquad \rho = 1.6 \times 10^{3}\ \mathrm{kg/m}^3,$$

where E is Young's modulus, A, the section area of truss member, and ρ, the mass density.

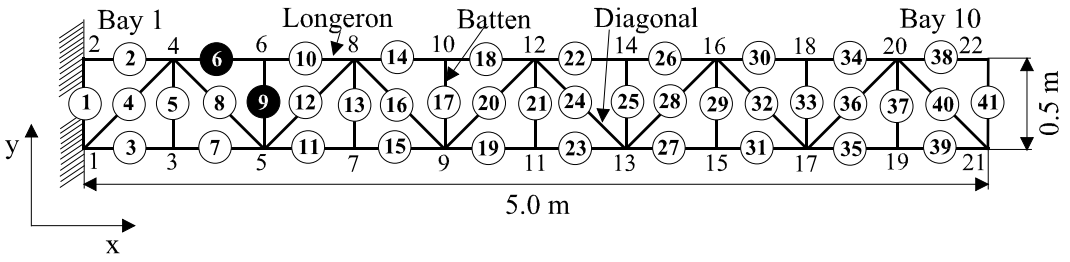

Fig. 1. A 10-bay planar truss structure for damage identification.

Table 1
Damage cases investigated for the planar truss

Damage case	Damaged strut	Damage condition
A	Element 6 in bay 2	10% reduction in E
B	Element 9 in bay 2	10% reduction in E
C	Element 6 in bay 2	50% reduction in E
D	Element 9 in bay 2	50% reduction in E
E	Elements 6 and 9 in bay 2	50% reduction in E

Three damage cases shown in Table 1 are investigated, including the longeron and batten damage cases. Also, all members in this truss are considered as damage candidates.

Firstly, for case A, the results of damage location detection using DDNKM and DDNK are illustrated in Fig. 2(a) and (b). From this figure, it can be found that both the approaches can identify the damaged strut effectively when only using first two modes. For the detection of damage location only, the Ritz approximation introduced in DDNKM has no obvious influence on accuracy. Another possible damaged strut is element 10, which is connected with the real damaged element from Fig. 1. By employing elements 6 and 10 as possible damaged struts, the damage extents of these two elements were evaluated. The results are shown in Table 2. It can be found that the damage extents predicted by DDNK are very accurate. Furthermore, only small deviation from the real damage extents can be identified for DDNKM, which means that the Ritz approximation is applicable for the lightly damaged cases. Also for both approaches, the undamaged strut in the possible candidates can be further detected effectively in this step. The above results demonstrate that the present methods appear to be promising for the longeron damage case.

For damage case B, the results of damage location are shown in Fig. 3(a) and (b). Inspection of this figure reveals that the damage location can be detected; however, the first three modes are needed. In this case, the real damaged element 9 can be identified uniquely. If only first two modes are employed, there are five possible damaged struts. In general, it is very difficult to detect the batten damage location since the battens usually only contribute to the high-order modes. The results of the damage extent are shown in Table 2. It can be found that the damage extent predicted by DDNK is exact; however, the accuracy of the damage extent estimated by DDNKM is a little lower than that in the longeron damage case.

For cases C and D, the results of damage detection using two approaches are identical to those of cases A and B shown in Figs. 2 and 3. For simplicity, these results are not illustrated again. It is reasonable by inspecting Eq. (19), where the influence of the damage extent can be eliminated absolutely. It is a

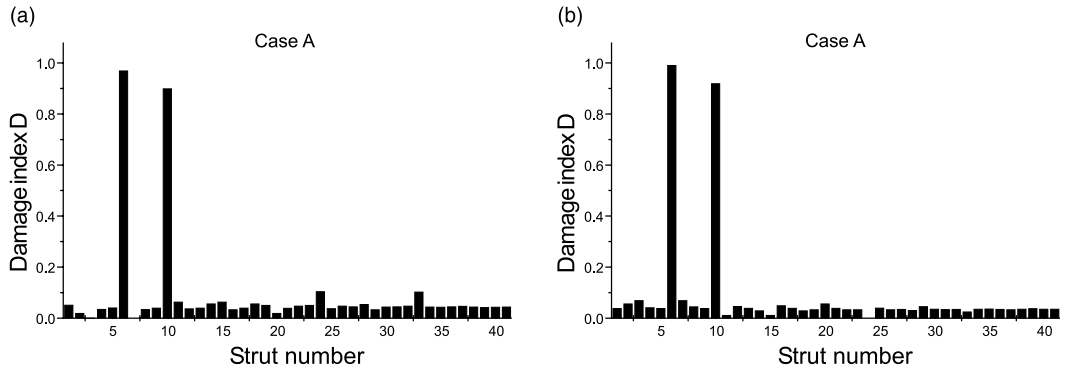

Fig. 2. Damage location results of damage case A using (a) DDNKM and (b) DDNK.

Table 2
Results of the damage extent for cases A–D

Damage case	Possible damaged strut	Number of modes used	Damage extent	
			DDNKM	DDNK
A	6, 10 (DDNKM) 6, 10 (DDNK)	1–2	0.109 (element 6) 0.000 (element 10)	0.100 (element 6) 0.000 (element 10)
B	9 (DDNKM), 9 (DDNK)	1–3	0.187 (element 9)	0.100 (element 9)
C	6, 10 (DDNKM) 6, 10 (DDNK)	1–2	0.906 (element 6) 0.000 (element 10)	0.500 (element 6) 0.000 (element 10)
D	9 (DDNKM), 9 (DDNK)	1–3	0.999 (element 9)	0.500 (element 9)

remarkable characteristic, which implies that the present technique may be very strong in the noisy situation. The predicted damage extents for cases C and D are shown in Table 2. Unlike cases A and B, the obtained damage extents from DDNKM for cases C and D are in great error. The incapability of the perturbation technique in DDNKM for heavily damaged cases is ascertained. The reason is that the Ritz approximation $\mathbf{\Phi}^* \approx \mathbf{\Phi\Gamma}$ introduces some great errors due to the significant difference inherited two modal spaces. The accuracy of the damage extent predicted by DDNKM will be promoted with the increase of the number of modes used in Ritz approximation. Generally, the prediction procedure of the damage extent in DDNKM may be profitable to locate the real damage site more clearly in spite of its inaccuracy in the damage extent by referring to case C. For DDNK, all results are accurate as shown in Table 2. From our numerical experiences, an important point is that, for both approaches, the accuracy in detection of damage location and prediction of damage extent becomes higher usually with the increase of the number of frequencies and modes.

For the multiple damage case E, the results of damage location obtained by employing the first three modes are shown in Fig. 4. Fig. 4(a) demonstrates that the damaged element 6 can be identified easily in the first step, and however, the damaged element 9 is concealed. This phenomenon is not strange, since element 6 dominates the lower-order vibration modes. By employing elements 6 and 10 as the possible damaged candidates, the damage extents were predicted. The results are shown in Table 3, in which the damage extent in element 6 can be predicted effectively, and the damage extent in element 10 is zero. By using the damage extent of element 6, the influence of element 6 can be eliminated in Eq. (29). Then, the detection of

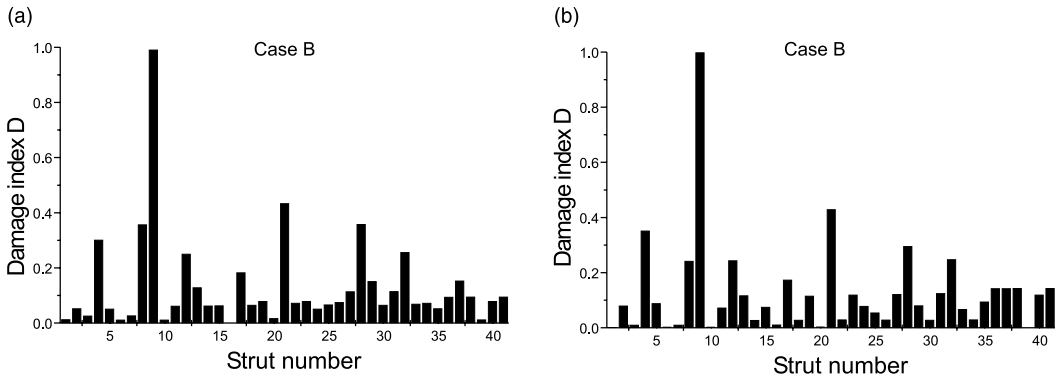

Fig. 3. Damage location results of damage case B using (a) DDNKM and (b) DDNK.

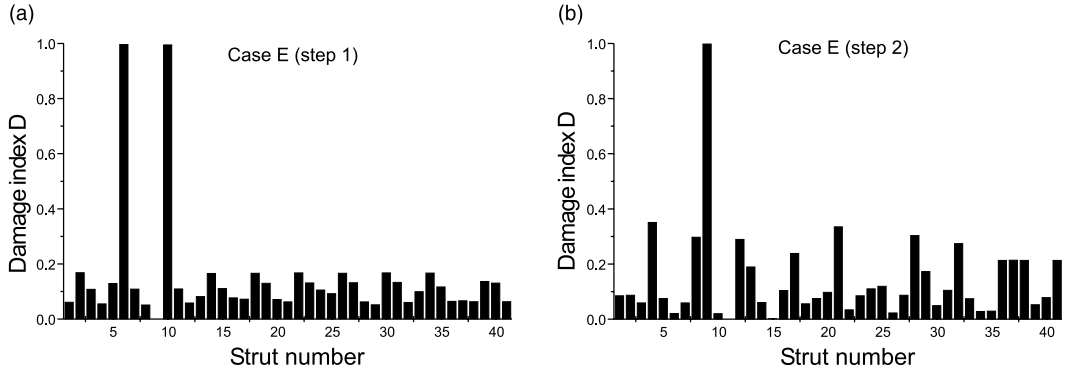

Fig. 4. Damage location results of damage case E using DDNK.

Table 3
Results of the damage extent for case E

Damage case	Possible damaged strut	Number of modes used	Damage extent (DDNK)
E	6, 10 (in step 1)	1–3	0.500 (element 6) 0.000 (element 10)
	9 (in step 2)	1–3	0.499 (element 9)

damage location can be performed again as the second step, which is shown in Fig. 4(b). Inspection of Fig. 4(b) reveals that element 9 can be detected uniquely. Its damage extent is listed in Table 3, which shows that the damage extent of element 9 can be calculated very accurately. However, for the multiple damage cases, our numerical experience shows that the careful selection modes is critical for the successful multiple damage identification. The same drawback may exist in some previous techniques, such as the minimum rank perturbation approach and eigenstructure assignment technique, which may require the optimal number of modes. Only one promising point from our numerical experiences is that the most structural critical or seriously damaged element, such as longerons in the present example, can always be detected in the first identification step.

3.2. Beam with two fixed ends

An aluminum beam with two fixed ends is used as the second example to validate the present theory experimentally. The material constants of the specimen are listed as follows:

$$E = 70 \text{ GPa}, \qquad \upsilon = 0.3, \qquad \rho = 2.70 \times 10^3 \text{ kg/m}^3.$$

The dimensions of the beam are shown in Fig. 5. A saw-cut damage was introduced by cutting two cracks on the top and bottom surface of the intact specimen as shown in Fig. 5. The depth of one crack is a quarter of the total thickness of the beam. Experimental modal analyses were conducted on intact and damaged specimens by employing an HP-5423A modal test device as shown in Fig. 6 and the impulse hammer input was used to excite the specimens. Only one accelerometer was employed at a reference point (center of the beam) for measuring the deflection response and the hammer input was acted at all points (marked by black circles in Fig. 5). The responses at all points were obtained through one line in the transfer function matrix, which was constructed using the hammer excitation and the FRF at the reference point. In HP-5423A, the

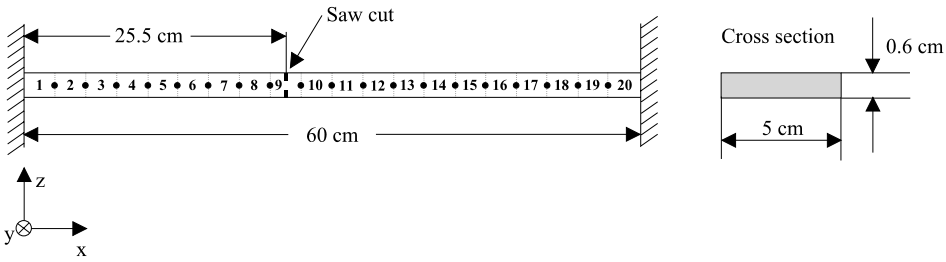

Fig. 5. A beam with two fixed ends.

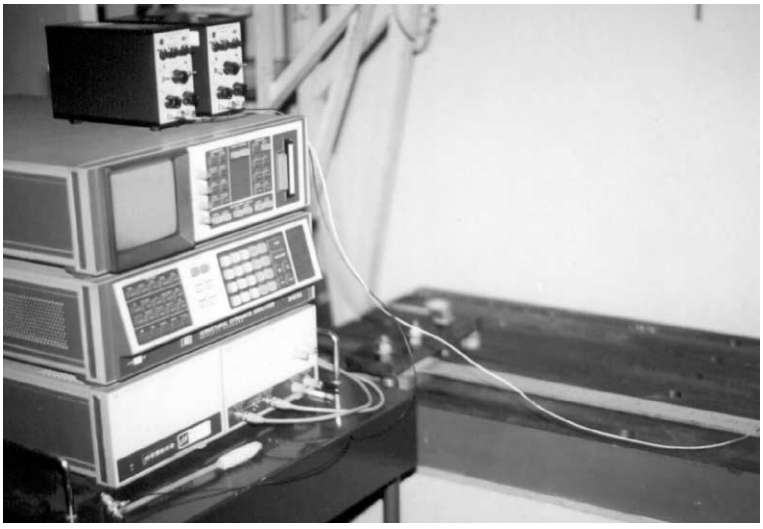

Fig. 6. Experimental instruments.

FRF was obtained by averaging the responses of six measurements. This technique is quite approximate due to the limited number of sensor. According to the requirement of Eq. (3), the mass-normalized modal shapes including deflection only at the points marked by '•' in Fig. 5 were outputted. Also, the FEM computation was performed employing 20 two-node beam elements, as shown in Fig. 5. The saw-cuts are located at the center of the ninth element. On one node of this element, there are two DOFs, i.e. deflection w and rotation θ_x. The saw-cut damage in the FEM computation is simulated using reduction of the bending rigidity in the ninth element, i.e. 87.5% reduction of I_y.

The first three-order frequencies of the intact and damaged beam are shown in Table 4. From this table, it can be found that the numerical results agree with the experimental ones very well for intact beam. However, the differences between the damaged practical and numerical models are greater. The measured first three-order mass-normalized modes (the unit of mode mass is $\mathrm{N\,s^2/cm}$) are plotted in Fig. 7. The modes obtained from the FEM analysis are also shown for comparison. From this figure, it can be found that the differences between the numerical and experimental modes is very significant, especially in the first mode, although the fundamental shapes are similar. The higher amplitudes in the experimental modes can be attributed to the following reasons: (1) imperfect fixation at two ends of beam allows the small rotations, (2) the approximate test technique due to only one sensor, (3) for this stiff metal structure, due to the low damping, the noise effect may be high, and (4) the numerical technique and assumed damage state in

Table 4
Results of the frequency for the beam with two fixed ends

	First frequency		Second frequency		Third frequency	
	Intact	Damaged	Intact	Damaged	Intact	Damaged
FEM	85.969	74.710	236.657	223.760	462.977	426.146
Experiment	85.726	83.984	238.572	235.792	467.694	462.712

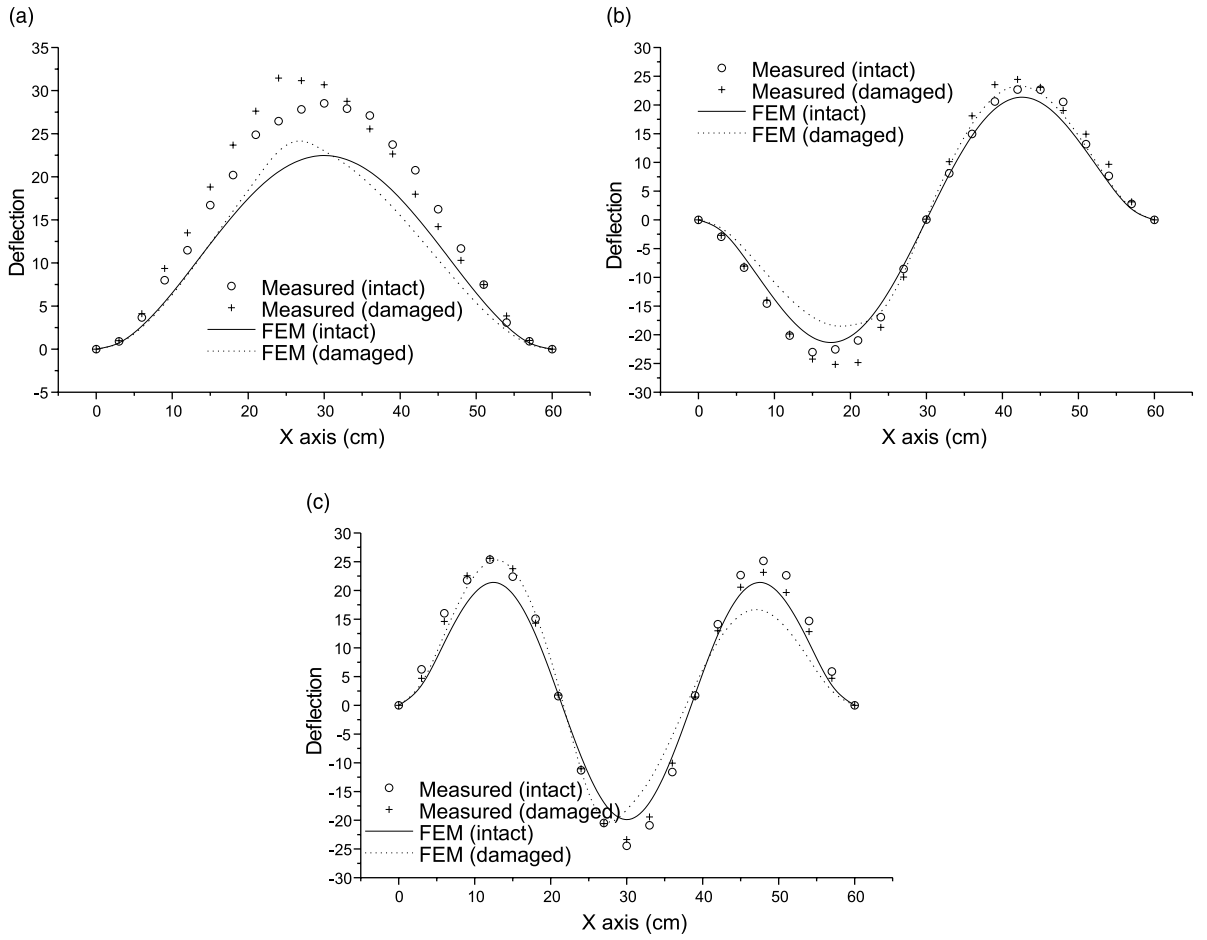

Fig. 7. Comparison of computational and experimental modes.

element 9 may result in the deviation. Although there are obvious differences in modal amplitudes, from Fig. 7(a), it can also be found that the positions of sudden change in slopes of two kinds of mode 1 are almost the same, i.e. in element 9. This feature is more important for detecting damages than that in the modal amplitude, since the reduction in bending rigidity is used for simulating damage. To carry out the damage identification, the rotations θ_x at the different nodes were obtained by differentiating the polynomial fitted curves from the measured deflections. This procedure may also lead to some errors. However, as stated previously, the position of sudden change in slope of modes is in element 9. Hence, it is possible for

us to get the reliable rotation data. It was found that the good results can be obtained when the order of the polynomial ranges from 6 to 9 from our practical experiences.

Actually, many authors have treated this damage detection problem for a beam. In many previous approaches, usually a baseline numerical model was set up first by modification of the original numerical model by using the test modal data. Then, based on this baseline model, the damage detection has been carried out. In this paper, we try to avoid using the numerical model. Hence, for checking the effectiveness of the present approaches, actually we have used a comparatively approximate experimental technique as stated previously and have not designedly pursued consistency between the experimental results and numerical ones. In fact, for complex structures, it is very hard to obtain a reasonable baseline model, and the test data are also inaccurate and limited. Naturally, without employing an effective baseline model, which can produce a similar modal data with the experimental ones, the damage detection becomes more difficult in the present approaches.

By employing the first two orders of measured modal data, the detection result using DDNKM is shown in Fig. 8(a). Although the damaged element 9 can be identified, the detection result is not so obvious due to the limited modal space in Eq. (5). The reason is that the Ritz approximation used in Eq. (4) introduces some great errors when the damage extent is high. The detection result of DDNK is shown in Fig. 8(b). It can be found that the damaged element 9 can be detected very clearly because Eq. (6) for DDNK is exact without using Ritz approximation. The damage extents of two approaches are listed in Table 5. From this table, it can be found that the damaged results obtained by DDNKM are in great error due to inaccurate Ritz approximation; however, the result of DDNK is better.

By employing the first three orders of measured modal data, the detection result using DDNKM is shown in Fig. 9(a). Inspection of Fig. 9(a) reveals that the damaged element 9 can be detected clearly,

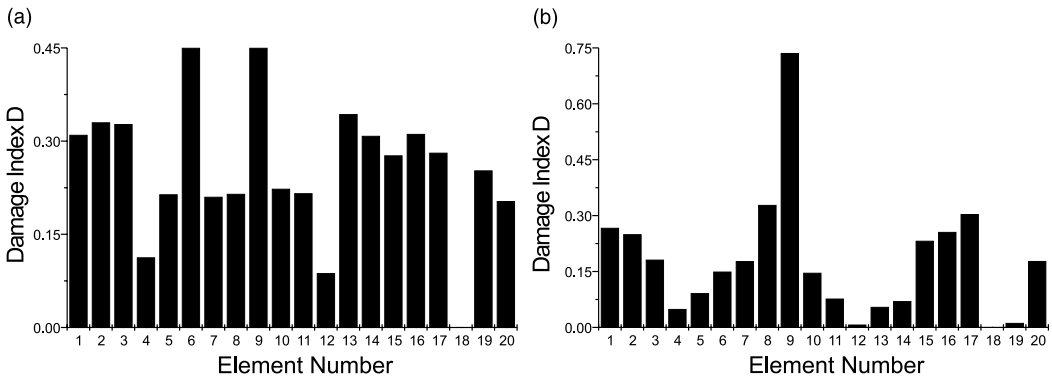

Fig. 8. Damage location results of the beam using the first two orders of modal data.

Table 5
Results of the damage extent for the beam with two fixed ends

Possible damaged strut	Number of modes used	Damage extent	
		DDNKM	DDNK
6, 9 (DDNKM)	1–2	0.882 (element 6)	
9 (DDNK)		0.323 (element 9)	0.582 (element 9)
8, 9 (DDNKM)	1–3	0.000 (element 8)	0.388 (element 8)
8, 9 (DDNK)		0.151 (element 9)	0.193 (element 9)

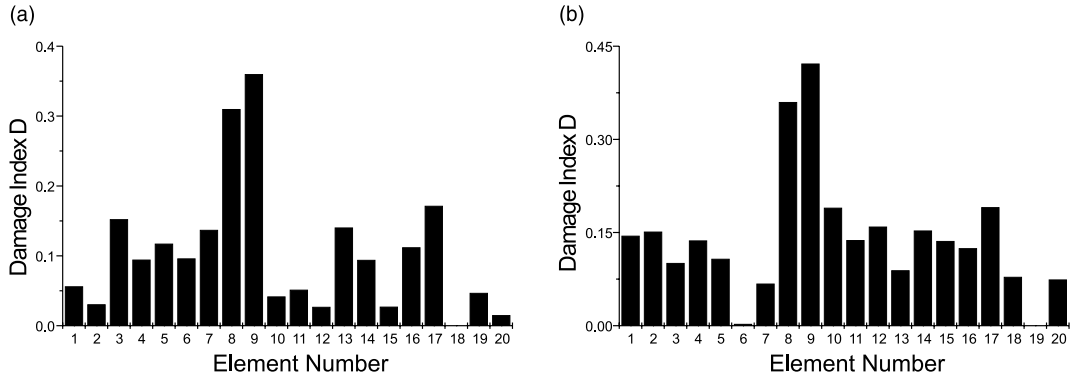

Fig. 9. Damage location results of the beam using the first three orders of modal data.

although the adjacent element 8 seems to be also damaged. Compared with Fig. 8(a), it can be found that the detection result becomes better. This phenomenon implies that the Ritz approximation used in DDNKM tend to be more accurate with the increase of the modal data. The detection result using DDNK is shown in Fig. 9(b). From this figure, it can be found that the damage location can also be identified. However, compared with Fig. 8(b), the detection result becomes a little worse due to the presence of the element 8 as a damaged one. The reasons may be from the assumed analytical mass, inaccurate rotations obtained from measured deflections, the noise included in the third mode caused by inaccurate measurement technique as stated previously. The damage extents are estimated by choosing elements 8 and 9 as the possible damaged members. The results of two approaches are shown in Table 5. From this table, it can be seen that there are great errors in the damage extents for two approaches. Also, compared with the results obtained by DDNK, the results obtained by DDNKM seem to be better, since the damage possibility of element 8 is excluded. Many factors can be attributed to this phenomenon, such as difference between the real mass and analytical mass models in DDNK, measured noises and the numerical element technique, etc.

4. Conclusions

In this paper, two damage identification approaches using relatively very little structural information and analytical global models have been developed. The first (DDNKM) does not employ the analytical global stiffness and mass matrices completely; the second one (DDNK) uses the analytical global mass matrix only. These approaches first locate the damages using a special subspace rotation algorithm, and then identify the magnitude of damage using the quadratic programming technique. They can locate the damaged element directly. As revealed by the numerical and experimental investigation, for the detection of damage location, both approaches work quite steadily. For the numerical example, DDNK can predict the accurate damage extent for different cases, but DDNKM can only tackle the lightly damaged cases. However, the experimental investigation shows that the accurate estimation of the damage extent is still a hard nut to crack.

Acknowledgements

This work was supported by Grant-Aid for International Cooperation Research No. 09044129 from the Ministry of Education, Science and Culture of Japan.

References

Chen, J.C., Garba, J.A., 1988. On-orbit damage assessment for large space structures. AIAA Journal 26 (12), 1119–1126.

Fukuanga, H., Sekine, H., Sasajima, K., Hu, N., Identification of damages in truss structures using vibration data. Transaction of the Japan Society of Mechanical Engineers, in press.

Goldfarb, D., Idnani, A., 1983. A numerically stable dual method for solving strictly convex quadratic programs. Mathematical Programming 27, 1–33.

Hajela, P., Soeiro, F.J., 1990. Recent developments in damage detection based on system identification methods. Structural Optimization 2 (1), 1–10.

Kahl, K., Sirkis, J.S., 1996. Damage detection in beam structures using subspace rotation algorithm with strain data. AIAA Journal 34 (12), 2609–2614.

Kaouk, M., Zimmerman, D.C., 1994. Structural damage assessment using a generalized minimum rank perturbation theory. AIAA Journal 32 (4), 836–842.

Lim, T.W., Kashangaki, T.A.-L., 1994. Structural damage detection of space truss structures using best-achievable eigenvectors. AIAA Journal 32 (5), 1049–1057.

Lim, T.W., 1995. Structural damage detection using constrained eigenstructure assignment. AIAA Journal of Guidance, Control and Dynamics 18 (3), 411–418.

Lin, C.S., 1995. Location of modeling errors using modal test data. AIAA Journal 28 (9), 1650–1654.

Pandey, A.K., Biswas, M., 1994. Damage detection in structures using changes in flexibility. Journal of Sound and Vibration 169 (1), 3–16.

Pandey, A.K., Biswas, M., Samman, M.M., 1991. Damage detection from changes in curvature mode shapes. Journal of Sound and Vibration 145 (2), 321–332.

Park, K.C., Alvin, K.F., 1996. A partitioned system identification procedure for substructural flexibility determination, AIAA Paper 96-1297.

Peterson, L.D., Doebling, S.W., Avlin, K.F., 1995. Experimental determination of local structural stiffness by disassembly of measured flexibility matrices. AIAA Paper 95-1090.

Ram, Y.M., Braun, S.G., 1991. An inverse problem associated with modification of incomplete dynamic systems. Journal of Applied Mechanics 58, 233–237.

Ricles, J.M., Kosmatka, J.B., 1992. Damage detection in elastic structures using vibratory residual forces and weighted sensitivity. AIAA Journal 30 (9), 2310–2316.

Zimmerman, D.C., Kaouk, M., 1992. Structural damage detection using a subspace rotation algorithm. Proceedings of the AIAA/ASME/ASCE/AHS/ASC 33rd Structures Structural Dynamics and Materials Conference, Dallas, USA.

Zimmerman, D.C., Smith, S.W., 1992. Model refinement and damage location for intelligent structures. In: Tzou, H.S., Anderson, G.L. (Eds.), Intelligent Structural Systems. Kluwer, Netherlands, pp. 403–452.